Effect of dimensionality on the percolation threshold of overlapping nonspherical hyperparticles

S. Torquato and Y. Jiao

Effect of Dimensionality on the Percolation Threshold of Overlapping Nonspherical Hyperparticles

S. Torquato*

Department of Chemistry, Department of Physics,
Princeton Institute for the Science and Technology of Materials,
and Program in Applied and Computational Mathematics, Princeton University, *Princeton NJ 08544*

Y. Jiao†

Princeton Institute for the Science and Technology of Materials, Princeton University, *Princeton NJ 08544*

In order to study the effect of dimensionality on the percolation threshold η_c of overlapping nonspherical convex hyperparticles with random orientations in d-dimensional Euclidean space $\mathbb{R}^d$, we formulate a scaling relation for η_c that is based on a rigorous lower bound [S. Torquato, J. Chem. Phys. **136**, 054106 (2012)] and a conjecture that hyperspheres provide the highest threshold among all convex hyperparticle shapes for any d. This scaling relation also exploits the recently discovered principle that low-dimensional continuum percolation behavior encodes high-dimensional information. We derive an explicit formula for the exclusion volume v_{ex} of a hyperparticle of arbitrary shape in terms of its d-dimensional volume v, surface area s and *radius of mean curvature* $\bar{R}$ (or, equivalently, *mean width*). These basic geometrical properties are computed for a wide variety of nonspherical hyperparticle shapes with random orientations across all dimensions, including, among other shapes, various polygons for $d = 2$, Platonic solids, spherocylinders, parallelepipeds and zero-volume plates for $d = 3$ and their appropriate generalizations for $d \geq 4$. Using this information, we compute the lower bound and scaling relation for η_c for this comprehensive set of continuum percolation models across dimensions. We demonstrate that the scaling relation provides accurate *upper-bound* estimates of the threshold η_c across dimensions and becomes increasingly accurate as the space dimension increases.

PACS numbers: 64.60.ah, 05.70.Jk, 71.30.+h, 82.70.Dd

I. INTRODUCTION

Clustering and percolation behavior of many-particle systems is of relevance in a host of physical and chemical phenomena, including gelation and polymerization, structure of liquids and glasses, hopping in semiconductors, metal-insulator transition in condensed matter systems, nucleation, condensation of gases, chemical association, conduction in dispersions, aggregation of colloids, and flow in porous media [1–6]. Considerable attention has been devoted to percolation on lattices, whose percolation thresholds, in some two-dimensional cases, are amenable to exact analysis [4, 5]. Unlike lattice percolation, it has not been possible to obtain exact results for the percolation threshold of any two-dimensional continuum (off-lattice) percolation model. Recently, analytical estimates of the threshold, including rigorous bounds, have been obtained for the prototypical continuum percolation models of overlapping hyperspheres and oriented hypercubes in d-dimensional Euclidean space $\mathbb{R}^d$ that apply in any dimension d [7, 8]. In this paper, we provide an analytical framework to predict percolation thresholds for a wide class of continuum percolation models, namely, overlapping hyperparticles in $\mathbb{R}^d$ of any convex shape and in any dimension d.

An important consequence of the analysis in Ref [7], which we exploit in the present work, is that the large-d percolation value for any hyperparticle shape is an important contribution to the corresponding low-dimensional percolation value. In other words, low-dimensional percolation properties encode high-dimensional information. The analysis was aided by a remarkable *duality* between the equilibrium hard-hypersphere (hypercube) fluid system and the continuum percolation model of overlapping hyperspheres (hypercubes), namely,

$$P(r; \eta) = -h(r; -\eta), \tag{1}$$

where $P(r; \eta)$ is the pair connectedness function at some radial distance r, the quantity

$$\eta = \rho v \tag{2}$$

---

*Electronic address: `torquato@princeton.edu`
†Electronic address: `yjiao@princeton.edu`

is a dimensionless or reduced density, ρ is the number density and v is the volume of a hyperparticle [9]. Additionally, $h(r; \eta)$ is the total correlation function for the corresponding equilibrium hard-particle models at *packing fraction η*, fraction of space covered by the hard particles. The duality relation (1) relates a statistical property of a topological problem on the one hand to that of a geometrical problem on the other [10]. Importantly, the duality relation (1) is exact in the large-d limit and for low densities for any d up to through the third virial level, and is a relatively accurate approximation in low dimensions for densities up to the percolation threshold η_c [7].

It was also shown in Ref. 7 that lower-order Padé approximants of the mean cluster number S of the form $[n, 1]$ (where $n = 0, 1$ and 2) provide upper bounds on S and hence yield corresponding lower bounds on the threshold η_c for d-dimensional overlapping hyperspheres and overlapping oriented convex hyperparticles with central symmetry [11] (e.g., spheres, cubes, regular octahedra, and regular icosahedra for $d = 3$) [7]. The simplest of these lower bounds on η_c ([0, 1] Padé approximant) is given by

$$\eta_c \geq \frac{1}{2^d}, \tag{3}$$

where it is to be noted that 2^d is the ratio of the exclusion volume v_{ex} associated oriented convex hyperparticle [12] (which includes the hypersphere) to the volume v of the hyperparticle. This trivially translates into a lower bound on the mean number of overlaps per sphere at the threshold $\mathcal{N}_c$:

$$\mathcal{N}_c \equiv 2^d \eta_c \geq 1. \tag{4}$$

The lower bound estimates as well as Percus-Yevick-like approximations were demonstrated [7] to become accurate in relatively low dimensions, improve in accuracy as d increases, and become asymptotically exact in the large-d limit, i.e.,

$$\eta_c \to \frac{1}{2^d}, \qquad d \to \infty \tag{5}$$

and

$$\mathcal{N}_c \sim 1, \qquad d \to \infty. \tag{6}$$

The aforementioned trends and asymptotic results were shown to hold for overlapping convex d-dimensional particles (or *hyperparticles*) of *arbitrary shape and orientational distribution* when appropriately generalized [7]. For example, for identical overlapping hyperparticles of general anisotropic shape of volume v with specified probability distribution of orientations in d dimensions, the simplest lower bound on η_c and on $\mathcal{N}_c$ generalize as follows:

$$\eta_c \geq \frac{v}{v_{\text{ex}}}, \tag{7}$$

$$\mathcal{N}_c \equiv \eta_c \frac{v}{v_{\text{ex}}} \geq 1, \tag{8}$$

where

$$v_{\text{ex}} = \int_{\mathbb{R}^d} f(\mathbf{r}, \boldsymbol{\omega}) p(\boldsymbol{\omega}) d\mathbf{r} d\boldsymbol{\omega}, \tag{9}$$

is the generalized *exclusion volume* associated with a hyperparticle, $f(\mathbf{r}, \boldsymbol{\omega})$ is the exclusion-region indicator function [7], $\mathbf{r}$ and $\boldsymbol{\omega}$ is the centroid position and orientation of one particle, respectively, with respect to a coordinate system at the centroid of the other particle with some fixed orientation, and $p(\boldsymbol{\omega})$ is the orientational probability density function. Moreover, in the high-dimensional limit for any convex hyperparticle shape, the following exact asymptotic results [15] immediately follow:

$$\eta_c \sim \frac{v}{v_{\text{ex}}}, \qquad d \to \infty \tag{10}$$

and

$$\mathcal{N}_c \sim 1, \qquad d \to \infty. \tag{11}$$

It was demonstrated in Ref. 7 that the lower bound (7) on η_c improves in accuracy in any fixed dimension as the particle shape becomes more anisotropic. This property will be exploited later in Sec. VI to obtain an upper bound on η_c.

We note that the bounds (7) and (8), and the associated asymptotic limits (10) and (11) also apply to overlapping *zero-volume* $(d-1)$-dimensional *hyperplates* with specified orientations in $\mathbb{R}^d$ when the relevant parameters are appropriately generalized. While these "infinitesimally thin" hyperplates in $\mathbb{R}^d$ have vanishing volumes, their exclusion volumes are nonzero at number density ρ. However, an appropriately defined "effective volume" v_{eff} must be chosen in order to define a reduced density η of the form (2) for hyperplates. The choice for this effective hyperplate volume that we use henceforth is the volume of a d-dimensional hypersphere of *characteristic radius* r, i.e.,

$$v_{\text{eff}} = \frac{\pi^{d/2}}{\Gamma(d/2+1)}r^d, \tag{12}$$

where r is related to some characteristic length scale of the hyperplate and $\Gamma(x)$ is the Euler-Gamma function. Thus, bounds (7) and (8) still apply for hyperplates when v in expression for the reduced density η is replaced by the effective volume (12), i.e.,

$$\eta_c \geq \frac{v_{\text{eff}}}{v_{\text{e}}}. \tag{13}$$

Application of the aforementioned continuum percolation results for nonspherical hyperparticles was only briefly explored in Ref. 7. The main objective of the present paper is to carry out such an investigation for a wide variety of nonspherical convex hyperparticles with *random orientations* across dimensions in order to ascertain the effect of dimensionality on the corresponding thresholds. This will be done by first ascertaining the exclusion volume of a wide variety of nonspherical hyperparticle shapes, and then applying the lower bound (7) on η_c and a scaling relation for η_c, the latter of which we obtain in the present paper.

All of the results described above reveal that the topological problem of percolation in low dimensions becomes a purely geometrical problem in high dimensions. This behavior is explicitly manifested by the duality relation (1) and the fact the threshold η_c is determined solely by the exclusion volume associated with a hyperparticle in the high-d limit [cf. (10)], a purely geometrical characteristic. Exploiting the latter result, the principle that low-dimensional results encode high-dimensional information [7], and a conjecture (postulated here) that hyperspheres provide the highest threshold among all convex hyperparticle shapes for any d, enables us to devise the aforementioned scaling relation for η_c for randomly oriented hyperparticles of general nonspherical shape, which is also shown to bound η_c from above.

The rest of the paper is organized as follows. In Sec. II, we derive an explicit formula for the exclusion volume v_{ex} associated with a nonspherical convex hyperparticle of arbitrary shape in terms of its basic geometrical properties. In Secs. III and IV, we compute these geometrical properties for a wide variety of nonspherical hyperparticle shapes with random orientations in two and three dimensions, and for $d \geq 4$. A conjecture that systems of overlapping hyperspheres provide the highest threshold among all convex hyperparticle shapes for any d is postulated in Sec. V. In Sec. VI, we derive a scaling relation for η_c and show that it is also an upper bound on η_c. In Sec. VII, we compute the lower bound (7) and scaling relation for η_c for the aforementioned comprehensive set of systems of overlapping hyperparticles and compare the results to numerical data for η_c, including those that we obtain here for the Platonic solids. Finally, in Sec. VIII, we close with concluding remarks.

II. EXCLUSION VOLUME FOR RANDOMLY ORIENTED OVERLAPPING NONSPHERICAL HYPERPARTICLES

The exclusion volume v_{ex} associated with randomly oriented overlapping convex nonspherical hyperparticles plays a central role in this paper. In what follows, we derive an explicit formula for v_{ex} in terms of the d-dimensional volume v, surface area s and *mean radius of mean curvature* $\bar{R}$ (or *mean width*) of a hyperparticle of arbitrary shape.

A. Basic Geometrical Characteristics of a Convex Body

Consider any convex body K in d-dimensional Euclidean space $\mathbb{R}^d$. Let v and s denote the d-dimensional volume and surface area of K, respectively. For example, in $\mathbb{R}^2$, v and s are the area and perimeter, respectively, of the two-dimensional convex body or disk. In Euclidean space $\mathbb{R}^d$, the parallel body associated with the convex body K at distance ϵ is equal to the sum of K and a Euclidean ball of diameter ϵ. This operation preserves the convexity and compactness properties associated with K. The notion of a parallel body or set is well known in convex geometry and has been applied in the physical sciences, even for non-convex geometries; see, for example, the so-called *dilation* processes that has been applied in the study of heterogeneous materials [5, 13, 14]. Figure 1 illustrates the parallel body associated with a rectangle in two dimensions.
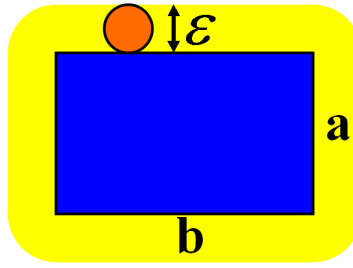
FIG. 1: (Color online) Two-dimensional illustration of the parallel body at a distance ϵ associated with a rectangle of side lengths a and b, which is the union of the blue (or dark gray) and yellow (or light gray) regions.
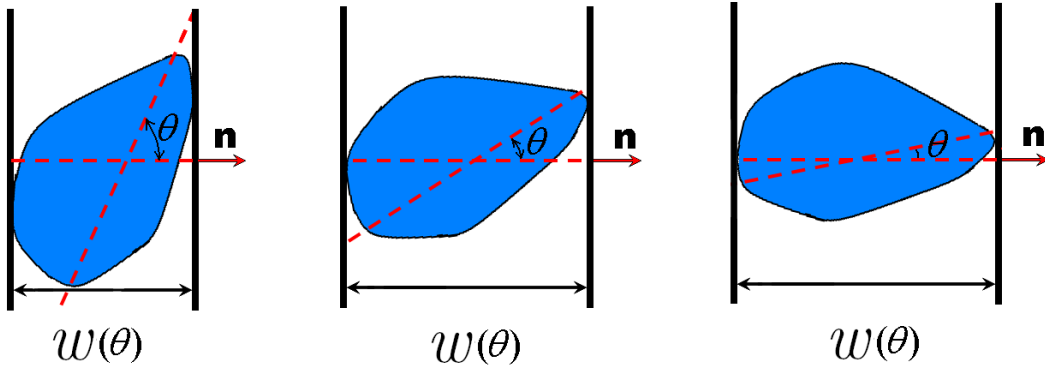

FIG. 2: (Color online) Illustration of the width w of a convex body in two dimensions. In $\mathbb{R}^2$, $w(\theta)$ is function of the angle θ between the normal $\mathbf{n}$ of the parallel planes (shown as red arrows) and the convex body. The mean with $\bar{w}$ is obtained by averaging $w(\theta)$ over the angle θ, i.e., integrating $w(\theta)$ over the angle θ and dividing by 2π.

The famous Steiner formula [17] expresses the volume of the parallel body v_ϵ at distance ϵ as a polynomial in ϵ and in terms of geometrical characteristics of the convex body K, such as v and s. For example, for the cases $d = 2$ and $d = 3$, Steiner's formula yields respectively

$$v_\epsilon = v + s\epsilon + \pi\epsilon^2 \tag{14}$$

and

$$v_\epsilon = v + s\epsilon + 4\pi\bar{R}\epsilon^2 + \frac{4\pi\epsilon^3}{3}, \tag{15}$$

where

$$\bar{R} = \frac{1}{8\pi} \int \left(\frac{1}{R_1} + \frac{1}{R_2} \right) dS, \tag{16}$$

is the *radius of mean curvature* of the convex body, R_1 and R_2 are the principle radii of curvature and dS denotes the integral over the entire surface of the convex body.

The Steiner formulas (14) and (15) can be generalized for a convex body K in any dimension d:

$$v_\epsilon = \sum_{k=0} W_k \epsilon^k, \tag{17}$$

where W_k are trivially related to the *quermassintegrals* or *Minkowski functionals* [17]. Note that $W_0 = v$, $W_1 = s$ and $W_d = v_s(d; \epsilon)$, where

$$v_s(d; a) = \frac{\pi^{d/2} a^d}{\Gamma(1 + d/2)} \tag{18}$$

is the volume of a d-dimensional sphere (hypersphere) of radius a. Of particular, interest in this paper is the *lineal* characteristic in (17), i.e., the $(d-1)$th coefficient:

$$W_{d-1} = \Omega(d)\bar{R}, \tag{19}$$

where

$$\Omega(d) = \frac{d\pi^{d/2}}{\Gamma(1+d/2)} \tag{20}$$

is the total solid angle contained in d-dimensional sphere and $\bar{R}$ is the radius mean of curvature in an space dimension d, which is trivially related to the *mean width* $\bar{w}$ of K via the following expression:

$$\bar{R} = \frac{\bar{w}}{2}. \tag{21}$$

The mean width $\bar{w}$ is a *lineal* (one-dimensional) measure of the "size" of K. Consider the convex body to be trapped entirely between two impenetrable parallel $(d-1)$-dimensional hyperplanes that are orthogonal to a unit vector $\mathbf{n}$ in $\mathbb{R}^d$. The "width" of a body $w(\mathbf{n})$ in the direction $\mathbf{n}$ is the distance between the closest pair of such parallel hyperplanes, implying that the hyperplanes contact the boundaries of the body. The mean width $\bar{w}$ is the average of the width $w(\mathbf{n})$ such that $\mathbf{n}$ is uniformly distributed over the unit sphere $S^{d-1} \in \mathbb{R}^d$. Figure 2 illustrates the concept of the width of a convex body in $\mathbb{R}^2$.

B. Explicit Formula for the d-Dimensional Exclusion Volume

General formulas for the exclusion volume associated with identical randomly oriented nonspherical convex particles in two and three dimensions have long been known [18, 19]. For example, for $d = 2$, it is known [18] that

$$v_{\text{ex}} = 2v + \frac{s^2}{2\pi} \tag{22}$$

where s is the two-dimensional surface area or *perimeter* of the convex body. Note that the first term of $2v$ is trivial, accounting for the fact that two bodies are excluding one another and hence the exclusion volume must be at least $2v$. At first glance, one might surmise that the appropriate three-dimensional expression for the exclusion volume involves a second term that is proportional to $s^{3/2}/(4\pi)$, where s is the surface area of the three-dimensional convex body. However, instead the correct three-dimensional formula [19] is

$$v_{\text{ex}} = 2v + \frac{sM}{2\pi}, \tag{23}$$

where

$$M = 4\pi\bar{R}. \tag{24}$$

The second terms in the two- and three-dimensional formulas (22) and (23), respectively, appear to be functionally distinct from one another. However, we will see shortly that by expressing both formulas in terms of $\bar{R}$ a unifying formula emerges that not only is valid for $d = 2$ and $d = 3$, but for arbitrary d.

To our knowledge, a formula for the exclusion volume associated with identical randomly oriented d-dimensional convex nonspherical bodies K for any d has heretofore not been given explicitly. We find that this exclusion volume is given by

$$v_{\text{ex}} = 2v + \frac{2(2^{d-1}-1)}{d}s\bar{R}. \tag{25}$$

We arrive at this general formula for any d by first recognizing that for the special case $d = 2$, the radius of mean curvature is trivially related to the two-dimensional surface area or perimeter, namely, $s = 2\pi\bar{R}$, which enables us to rewrite relation (22) as follows:

$$v_{\text{ex}} = 2v + s\bar{R}. \tag{26}$$

Similarly, using Eq. (24), we can re-express relation (23) for $d = 3$ in terms of $\bar{R}$, namely,

$$v_{\text{ex}} = 2v + 2s\bar{R}. \tag{27}$$

We see that these two- and three-dimensional formulas differ by a coefficient multiplying the product $s\bar{R}$, independent of the shape of the convex body. Assuming that this coefficient depends only on dimension, the general d-dimensional formula for v_{ex} associated with any convex body K must have the form

$$v_{\mathrm{ex}} = 2v + C(d)s\bar{R}, \qquad (28)$$

where $C(d)$ is a d-dimensional coefficient that still must be determined. To determine $C(d)$ as a function of d, we exploit the assumption that (28) must apply to any convex body so that one can use the most convenient shape, i.e., a d-dimensional sphere (hypersphere). Note that the dimensionless exclusion volume v_{ex}/v of a hypersphere, among all convex hyperparticles of nonzero volume, takes on its *minimum* value of 2^d [7]. For a hypersphere of radius a, the volume v is given by (18), $\bar{R} = a$, and the surface area is given by

$$s_s(d;a) = \frac{d\pi^{d/2}}{\Gamma(1 + \frac{d}{2})}a^{d-1}. \qquad (29)$$

Using these last four geometrical-property relations in conjunction with formula (28) yields

$$C(d) = \frac{2^d - 2}{d}. \qquad (30)$$

Substitution of this expression into relation (28) gives the general relation (25) for the exclusion volume.

We now show that the general formula (25) is indeed exact for any d. Using relation (25) and the fact that v_{ex}/v is minimized for hyperspheres (with $v_{\mathrm{ex}}/v = 2^d$) among all convex hyperparticles of nonzero volume, we can obtain the following inequality involving s, $\bar{R}$ and v;

$$s\bar{R} \geq dv, \qquad (31)$$

where the equality holds for hyperspheres only. This bound is a type of *isoperimetric inequality* and has been proved in the study of convex geometry using completely different techniques [20]. The fact that the general expression (25) for v_{ex} independently leads to a rigorously proven isoperimetric inequality for any convex body in $\mathbb{R}^d$ clearly justifies our assumptions concerning the form (28) and indirectly proves that (25) is an exact formula for any convex body in $\mathbb{R}^d$. Moreover, we have computed v_{ex}/v for a hypercube in $\mathbb{R}^4$ using Monte-Carlo simulations and verified that the numerical value agrees very well with the analytical result given by (25), as expected.

Note that for $d = 2$, inequality (31) yields the standard isoperimetric inequality $s \geq 4\pi v$, where we have used the fact that the surface or perimeter $s = 2\pi\bar{R}$. The d-dimensional generalization of this standard isoperimetric inequality is

$$s\,\Omega(d)^d \geq dv^{\frac{d-1}{d}}, \qquad (32)$$

where $\Omega(d)$ is given by (20) [20]. It is clear that this inequality is not the same as (31).

We see that in the case that a $(d-1)$-dimensional convex *hyperplate* in $\mathbb{R}^d$ that possesses zero volume, i.e., $v = 0$, the exclusion-volume formula (25) yields

$$v_{\mathrm{ex}} = \frac{2(2^{d-1} - 1)}{d}s\bar{R}. \qquad (33)$$

We shall consider examples of such convex bodies for $d \geq 3$ in the subsequent section.

III. RADII OF MEAN CURVATURE AND EXCLUSION VOLUMES FOR VARIOUS NONSPHERICAL PARTICLES IN TWO AND THREE SPACE DIMENSIONS

Here we present results for the aforementioned geometrical characteristics of a variety of convex bodies that are randomly oriented in two and three dimensions possessing both nonzero and zero volumes. In the former instance, it is convenient to consider the dimensionless exclusion volume v_{ex}/v. Two- and three-dimensional exclusion volumes are known for a variety of convex nonspherical shapes that are randomly oriented [18, 19]. It necessarily follows that such exclusion volumes are larger than the corresponding values when all of the particles are aligned and centrally symmetric, in which case $v_{\mathrm{ex}}/v_1 = 2^d$, independent of the particle shape [7].

A. Two Dimensions

Table I provides volumes, surface areas, radii of mean curvature, and exclusion volumes for some two-dimensional convex particles. This includes the circle, certain regular polygons, rectangle, spherocylinder and ellipse. The exclusion volumes for these particles are easily be obtained from relation (22). Alternatively, the radius of mean curvature $\bar{R}$ can be obtained from the volume of the parallel body associated with the convex body at distance ϵ that is of order ϵ and use of relation (19). The corresponding exclusion volume can then be found employing relation (25) for $d = 2$.

In the "needle-like" limit for an ellipse ($b/a \to \infty$), the general quantities $\bar{R}$ and v_{ex}/v given in Table I become

$$\bar{R} \sim \frac{2b}{\pi}, \qquad \frac{v_{\text{ex}}}{v} \sim \frac{8}{\pi^2} \frac{b}{a}, \qquad b/a \to \infty. \tag{34}$$

The radius of mean curvature for a randomly oriented, zero-volume *lines* of length a in $\mathbb{R}^2$ is easily obtained from the rectangular case in Table I with $a_1 = 0$ and $a_2 = a$, yielding

$$\bar{R} = \frac{a}{\pi} \qquad \text{(line)}. \tag{35}$$

The corresponding exclusion volume is extracted from Table I in the rectangular case by first multiplying both sides of the relation for v_{ex}/v by the volume $v = ab$, and then setting $a_1 = 0$ and $a_2 = a$, which gives

$$v_{\text{ex}} = \frac{2a}{\pi} \qquad \text{(line)}. \tag{36}$$

Not surprisingly, $\bar{R}$ for a line of length a is identical to that of a needle-like ellipse of major axis $2b = a$ [cf. (34)].

TABLE I: Volumes, surface areas, radii of mean curvature, and exclusion volumes for some convex particles K in $\mathbb{R}^2$. The radius of mean curvature and exclusion volume correspond to randomly oriented convex particles having nonzero volumes.

K	v	s	$\bar{R}$	v_{ex}/v
Circular disk, radius a	πa^2	$2\pi a$	a	4
Octagon, side a	$2(1+\sqrt{2})a^2$	$8a$	$\frac{4a}{\pi}$	$2 + \frac{16}{\pi(1+\sqrt{2})}$
Hexagon, side a	$\frac{\sqrt{3}a^2}{4}$	$6a$	$\frac{3a}{\pi}$	$2 + \frac{4\sqrt{3}}{\pi}$
Pentagon, side a	$\frac{\sqrt{25+10\sqrt{5}}a^2}{4}$	$3a$	$\frac{5a}{2\pi}$	$2 + \frac{50}{\pi\sqrt{25+10\sqrt{5}}}$
Square, side a	a^2	$4a$	$\frac{2a}{\pi}$	$2 + \frac{8}{\pi}$
Equilateral triangle, side a	$\frac{\sqrt{3}a^2}{4}$	$3a$	$\frac{3a}{2\pi}$	$2 + \frac{6\sqrt{3}}{\pi}$
Rectangle, sides a_1, a_2	$a_1 a_2$	$2(a_1 + a_2)$	$\frac{a_1+a_2}{\pi}$	$2 + \frac{2(a_1+a_2)^2}{a_1 a_2 \pi}$
Spherocylinder, radius a cylindrical height h	$\pi a^2 + 2ah$	$2(\pi a + h)$	$\frac{h}{\pi} + a$	$2 + \frac{2(\pi a + h)^2}{\pi a(\pi a + 2h)}$
Ellipse, semiaxis a semiaxis $b \geq a$	πab	$4bE(\sqrt{1-\frac{a^2}{b^2}})$	$\frac{2b}{\pi}E(\sqrt{1-\frac{a^2}{b^2}})$	$2 + \frac{8b}{\pi^2 a}E^2(\sqrt{1-\frac{a^2}{b^2}})$

B. Three Dimensions

Table II provides volumes, surface areas, radii of mean curvature, and exclusion volumes for some three-dimensional convex particles. This includes the sphere, Platonic solids, rectangular parallelepiped, spherocylinder and spheroid. The radius of mean curvature $\bar{R}$ can be obtained from the volume of the parallel body associated with the convex body at distance ϵ that is of order ϵ^2 and use of relation (19). The corresponding exclusion volume can then be found employing relation (25) for $d = 3$.

It is easy to extract $\bar{R}$ and v_{ex}/v from the spheroid results in Table II the "prolate-needle" ($b/a \to \infty$) and "oblate-needle" ($b/a \to 0$) limits, which are respectively given by

$$\bar{R} \sim \frac{b}{2}, \qquad \frac{v_{\text{ex}}}{v} \sim \frac{3\pi}{4} \frac{b}{a}, \qquad b/a \to \infty, \tag{37}$$

and

$$\bar{R} \sim \frac{\pi}{4}a, \qquad \frac{v_{\text{ex}}}{v} \sim \frac{3\pi}{4}\frac{a}{b}, \qquad b/a \to 0. \tag{38}$$

TABLE II: Volumes, surface areas, radii of mean curvature, and exclusion volumes for some convex particles K in $\mathbb{R}^3$. The radius of mean curvature and exclusion volume correspond to randomly oriented convex particles having nonzero volumes.

K	v	s	$\bar{R}$	v_{ex}/v
Sphere, radius a	$\frac{4\pi a^3}{3}$	$4\pi a^2$	a	8
Icosahedron, side a	$\frac{5}{12}(3+\sqrt{5})a^3$	$5\sqrt{3}a^2$	$\frac{30}{8\pi}\cos^{-1}(\frac{\sqrt{5}}{3})a$	$2+\frac{90\sqrt{3}\cos^{-1}(\frac{\sqrt{5}}{3})}{\pi(3+\sqrt{5})}$
Dodecahedron, side a	$\frac{15+7\sqrt{5}}{4}a^3$	$3\sqrt{25+10\sqrt{5}}a^2$	$\frac{30}{8\pi}\cos^{-1}(\frac{1}{\sqrt{5}})a$	$2+\frac{90\sqrt{25+10\sqrt{5}}\cos^{-1}(\frac{1}{\sqrt{5}})}{\pi(15+7\sqrt{5})}$
Cube, side a	a^3	$6a^2$	$\frac{3a}{4}$	11
Octahedron, side a	$\frac{\sqrt{2}}{3}a^3$	$2\sqrt{3}a^2$	$\frac{3}{2\pi}\cos^{-1}(\frac{1}{3})a$	$2+\frac{9}{\pi}\sqrt{\frac{3}{2}}\cos^{-1}(\frac{1}{3})$
Tetrahedron, side a	$\frac{\sqrt{2}}{12}a^3$	$\sqrt{3}a^2$	$\frac{3}{4\pi}\cos^{-1}(-\frac{1}{3})a$	$2+\frac{18}{\pi}\sqrt{\frac{3}{2}}\cos^{-1}(-\frac{1}{3})$
Rectangular parallelpiped sides a_1, a_2, a_3	$a_1 a_2 a_3$	$\sum_{i<j}^{3}2a_i a_j$	$\frac{1}{4}\sum_{i=1}^{3}a_i$	$2+\frac{(\sum_{i<j}^{3}a_i a_j)(\sum_{i=1}^{3}a_i)}{a_1 a_2 a_3}$
Cylinder, radius a height h	$\pi a^2 h$	$2\pi a(a+h)$	$\frac{\pi a+h}{4}$	$2+\frac{(a+h)(\pi a+h)}{2ah}$
Spherocylinder, radius a cylindrical height h	$\frac{\pi a^2(4a+3h)}{3}$	$2\pi a(2a+h)$	$\frac{h+4a}{4}$	$2+\frac{3(2a+h)(4a+h)}{a(4a+3h)}$
Prolate spheroid semiaxes $a=c$, $b \geq a$ $e^2 = 1-(a/b)^2$	$\frac{4\pi a^2 b}{3}$	$2\pi a^2\big(1+\frac{b}{ae}\sin^{-1}e\big)$	$\frac{b}{2}\big(1+\frac{a^2}{b^2 e}\tanh^{-1}e\big)$	$2+\frac{3}{2}\big(1+\frac{b}{ae}\sin^{-1}e\big)$ $\times\big(1+\frac{a^2}{b^2 e}\tanh^{-1}e\big)$
Oblate spheroid semiaxes $a=c$, $b \leq a$ $e^2 = 1-(b/a)^2$	$\frac{4\pi a^2 b}{3}$	$2\pi a^2\big(1+\frac{b^2}{a^2 e}\tanh^{-1}e\big)$	$\frac{b}{2}\big(1+\frac{a}{be}\sin^{-1}e\big)$	$2+\frac{3}{2}\big(1+\frac{b^2}{a^2 e}\tanh^{-1}e\big)$ $\times\big(1+\frac{a}{be}\sin^{-1}e\big)$

Table III provides surface areas, radii of mean curvature, and exclusion volumes for some three-dimensional convex plates. This includes the circular, square, equilateral triangular, rectangular and elliptical plates. The radius of mean curvature $\bar{R}$ can be easily obtained from the volume of the parallel body associated with the convex body at distance ϵ that is of order ϵ^2 and use of relation (19). The corresponding exclusion volume can then be found using relation (25) for $d=3$. Alternatively, in the cases of circular, square and rectangular plates, $\bar{R}$ and v_{ex} can be obtained from Table II as special cases of the cylinder (when $h=0$) and rectangular parallelpiped ($a_1 = a_2 = a$, $a_3 = 0$ for the square plate and $a_3 = 0$ for the rectangular plate). To get v_{ex} in these cases, one must first multiply v_{ex}/v in Table II by the volume v and then take the aforementioned limits.

TABLE III: Surface areas, radius of mean curvature, and exclusion volumes for some convex plates K in $\mathbb{R}^3$ possessing a volume $v=0$. The radius of mean curvature and exclusion volume correspond to randomly oriented convex plates.

K	s	$\bar{R}$	v_{ex}
Circular plate, radius a	$2\pi a^2$	$\frac{\pi}{4}a$	$\pi^2 a^3$
Square plate, side a	$2a^2$	$\frac{1}{2}a$	$2a^3$
Equilateral triangular plate, side a	$\frac{\sqrt{3}}{2}a^2$	$\frac{3}{8}a$	$\frac{3\sqrt{3}}{8}a^3$
Rectangular plate, sides a_1, a_2	$2a_1 a_2$	$\frac{1}{4}(a_1+a_2)$	$a_1 a_2(a_1+a_2)$
Elliptical plate, semiaxis a semiaxis $b \geq a$	$2\pi ab$	$\frac{1}{2}bE(\sqrt{1-a/b}\,)$	$2\pi ab^2 E(\sqrt{1-a/b}\,)$

IV. RADII OF MEAN CURVATURE AND EXCLUSION VOLUMES FOR VARIOUS HYPERPARTICLES

We present here explicit formulas for the radii of mean curvature and exclusion volumes for a variety of hyperparticles in $\mathbb{R}^d$ with random orientations possessing both nonzero and zero volumes (hyperplates).

A. Hypercube and Hyperrectangular Parallelpiped

1. Hypercube

The determination of the radius of mean curvature $\bar{R}$ for a d-cube (hypercube) of edge (or side) length a is easily obtained from the d-dimensional generalization of Steiner's formula. Associated with the ϵ neighborhood of an edge is a portion of a $(d-1)$-dimensional hypercylinder of height a and radius ϵ, the volume of which is given by

$$v_{\mathrm{cyl}} = v_s(d-1;\epsilon)\, a = \frac{\pi^{(d-1)/2}}{\Gamma(1+\frac{d-1}{2})}\, a\,\epsilon^{d-1}, \tag{39}$$

where $v_s(d;a)$ is the volume of a d-dimensional hypersphere of radius a explicitly given by (18). Hence, the volume associated with a hypercube edge is $v_{\mathrm{cyl}}/2^{d-1}$. Since a hypercube has a total of $d2^{d-1}$ edges, the total volume associated with all of the edges is dv_{cyl}. Therefore, equating this volume with the term $W_{d-1}\epsilon^{d-1}$ in Steiner's formula (17) and using (19) yields

$$\Omega(d)\bar{R}\epsilon^{d-1} = dv_{\mathrm{cyl}}, \tag{40}$$

and hence the radius of mean curvature for a hypercube of side length a is given by

$$\bar{R} = \frac{\Gamma(1+\frac{d}{2})}{\sqrt{\pi}\Gamma(\frac{d+1}{2})}\, a. \tag{41}$$

For large d, we obtain the asymptotic result

$$\bar{R} \sim \sqrt{\frac{d}{2\pi}}, \qquad d \to \infty. \tag{42}$$

Not surprisingly, for large d, the longest diagonal, which grows like $\sqrt{d}$, is the dominant contribution to $\bar{R}$.

Using Eqs. (25) and (41) and the fact that the surface area of a hypercube of side length a are given by $s = 2d\,a^{d-1}$ and $v = a^d$, respectively, we obtain the following expression for the exclusion volume:

$$\frac{v_{\mathrm{ex}}}{v} = 2 + \frac{4(2^{d-1}-1)}{\sqrt{\pi}}\frac{\Gamma(1+\frac{d}{2})}{\Gamma(\frac{d+1}{2})}. \tag{43}$$

In the large-d limit, this expression and (42) yield the asymptotic result

$$\frac{v_{\mathrm{ex}}}{v} \sim \sqrt{\frac{2d}{\pi}}\, 2^d, \qquad d \to \infty. \tag{44}$$

2. Hyperrectangular Parallelpiped

Consider a d-rectangular parallelpiped (hyperrectangular parallelpiped) with edges of side lengths $a_1, a_2, \cdots, a_d$. Using a similar analysis as for the hypercube, we find the radius of mean curvature is given by

$$\bar{R} = \frac{\Gamma(1+\frac{d}{2})}{d\sqrt{\pi}\,\Gamma(\frac{d+1}{2})}\, \sum_{i=1}^{d} a_i. \tag{45}$$

Employing Eqs. (25) and (45) and the fact that the surface area of a hyperrectangular parallelpiped of side lengths $a_1, a_2, \ldots, a_d$ is given by $s = \sum_{i<j<k<l\ldots}^{d} 2a_i a_j a_k a_l \cdots$ (where $a_i a_j a_k a_l \cdots$ is the product of $d-1$ different side lengths) and $v = \prod_{i=1}^{d} a_i$, we obtain the following expression for the exclusion volume:

$$\frac{v_{\text{ex}}}{v} = 2 + \frac{2(2^{d-1}-1)}{d^2\sqrt{\pi}} \frac{\Gamma(1+\frac{d}{2})}{\Gamma(\frac{d+1}{2})} \frac{\left(\sum_{i<j<k<l\cdots}^{d} 2a_i a_j a_k a_l \cdots\right)\left(\sum_{i=1}^{d} a_i\right)}{\prod_{i=1}^{d} a_i}. \tag{46}$$

Consider the special case in which there are $d-1$ edges with side length a and the remaining edge with side length b. Then, formulas (45) and (46) simplify as follows:

$$\bar{R} = \frac{\Gamma(1+\frac{d}{2})}{\sqrt{\pi}d\,\Gamma(\frac{d+1}{2})}[(d-1)a+b]\,, \tag{47}$$

$$\frac{v_{\text{ex}}}{v} = 2 + \frac{4(2^{d-1}-1)}{d^2\sqrt{\pi}} \frac{\Gamma(1+\frac{d}{2})}{\Gamma(\frac{d+1}{2})}\left[(d-1)\frac{b}{a}+1\right]\left[(d-1)\frac{a}{b}+1\right]. \tag{48}$$

We shall subsequently make use of these relations in deriving certain hyperplate results.

B. Hyperspherocylinder

Consider a d-spherocylinder (hyperspherocylinder) of height h and radius a, which can be decomposed into hypercylinder of height h and two hemispherical caps of radius a (i.e., hypersphere of radius a). The volume of order ϵ^{d-1} associated with the ϵ neighborhood of a hyperspherocylinder is

$$\frac{\pi^{(d-1)/2}\epsilon^{d-1}h}{\Gamma(\frac{d+1}{2})} + \frac{\pi^{d/2}d\epsilon^{d-1}a}{\Gamma(1+d/2)},$$

which when equated with the term $W_{d-1}\epsilon^{d-1}$ in Steiner's formula (17) and using (19) gives

$$\Omega(d)\bar{R}\epsilon^{d-1} = \frac{d\pi^{(d-1)/2}\epsilon^{d-1}h}{\Gamma(\frac{d+1}{2})} + \frac{\pi^{d/2}d\epsilon^{d-1}a}{\Gamma(1+d/2)}, \tag{49}$$

and hence the radius of mean curvature for a hyperspherocylinder is given by

$$\bar{R} = \frac{\Gamma(1+\frac{d}{2})}{d\sqrt{\pi}\,\Gamma(\frac{d+1}{2})}\,h + a. \tag{50}$$

For large d, we find the asymptotic result

$$\bar{R} \sim \sqrt{\frac{1}{2\pi d}}\,h + a, \qquad d \to \infty. \tag{51}$$

We see that if h grows mores slowly with dimension than $\sqrt{d}$,

$$\bar{R} \sim a, \qquad d \to \infty. \tag{52}$$

The surface area and volume of a spherocylinder are given respectively by

$$s = s_s(d-1;a)h + s_s(d;a) \tag{53}$$

and

$$v = v_s(d-1;a)h + v_s(d;a), \tag{54}$$

where $s_s(d;a)$ and $v_s(d;a)$ are the surface area of a d-dimensional hypersphere of radius a given by (29) and (18), respectively. These relations combined with Eqs. (25) and (50) yield the exclusion volume to be given by

$$\frac{v_{\mathrm{ex}}}{v} = 2 + \frac{2(2^{d-1}-1)}{d}\left[\frac{s_s(d-1;a)h + s_s(d;a)}{v_s(d-1;a)h + v_s(d;a)}\right]\left[\frac{\Gamma(1+\frac{d}{2})h}{d\sqrt{\pi}\,\Gamma(\frac{d+1}{2})} + a\right]. \tag{55}$$

In the large-d limit, this relation yields the asymptotic result

$$\frac{v_{\mathrm{ex}}}{v} \sim \left[\frac{h}{a}\sqrt{\frac{1}{2\pi d}} + 1\right]2^d, \tag{56}$$

where we have used (51). We observe that in order for the contribution to the the scaled exclusion volume from the cylindrical portion, first term in (56), not to vanish as d becomes large, the aspect ratio h/a must grow as fast as $\sqrt{d}$ or faster.

C.   Hyperoctahedron and Hypertetrahedron

A regular d-crosspolytope or regular hyperoctahedron (also known as the orthoplex) is the d-dimensional generalization of the three-dimensional regular octahedron. For $d = 1$ and $d = 2$, the regular hyperoctahedron is a line and square, respectively. A regular d-simplex or hypertetrahedron is the d-dimensional generalization of the three-dimensional regular tetrahedron. For $d = 1$ and $d = 2$, the regular hypertetrahedron is a line and equilateral triangle, respectively. For $d \geq 5$, there are only three types of convex regular polytopes: the regular hypercube, hyperoctahedron and hypertetrahedron [21]. For a regular hyperoctahedron and regular hypertetrahedron, the radius of mean curvature is not as easy to derive from Steiner's formula, but integral formulas for it have been derived [22–24].

1.   Regular Hyperoctahedron (d-Crosspolytope)

For a regular hyperoctahedron with unit side length, the radius of mean curvature is given by [23, 24]

$$\bar{R} = \frac{\sqrt{2}\,d(d-1)\,\Gamma(\frac{d}{2})}{2\sqrt{2}\pi\Gamma(\frac{d+1}{2})}\,I_O(d), \tag{57}$$

where

$$I_O(d) = \int_0^\infty \exp(-2x^2)\,\mathrm{erf}(x)^{d-2}\,dx. \tag{58}$$

Note that for $d = 2$ and $d = 3$, we respectively have

$$I_O(2) = \frac{\sqrt{\pi}}{2\sqrt{2}} \tag{59}$$

and

$$I_O(3) = \frac{1}{\sqrt{2\pi}}\tan^{-1}(\frac{1}{\sqrt{2}}). \tag{60}$$

Substitution of these formulas into (57) recovers the results for $\bar{R}$ listed in Tables I and II for the square and octahedron, respectively. For large d, it is straightforward to show that

$$I_O(d) \sim \frac{\pi\sqrt{\ln d}}{2d^2}, \tag{61}$$

which implies

$$\bar{R} \sim \sqrt{\frac{\ln d}{d}}, \qquad d \to \infty. \tag{62}$$

The surface area and volume of a regular hyperoctahedron are given respectively by

$$s = \frac{2^{(d+1)/2}\sqrt{d}}{(d-1)!} \tag{63}$$

and

$$v = \frac{2^{d/2}}{d!}. \tag{64}$$

These relations combined with Eqs. (25) and (57) yield the exclusion volume to be given by

$$\frac{v_{\text{ex}}}{v} = 2 + \frac{4d^{3/2}(d-1)\,\Gamma(\frac{d}{2})(2^{d-1}-1)}{\pi\Gamma(\frac{d-1}{2})}I_O(d). \tag{65}$$

In the large-d limit, this relation and (62) give the asymptotic result

$$\frac{v_{\text{ex}}}{v} \sim \sqrt{2\ln(d)}\,2^d, \qquad d \to \infty. \tag{66}$$

2. Regular Hypertetrahedron (d-Simplex)

For a regular hypertetrahedron with unit side length, the radius of mean curvature is given by [22, 24]

$$\bar{R} = \frac{d(d+1)\,\Gamma(\frac{d}{2})}{2\sqrt{2}\,\pi\Gamma(\frac{1+d}{2})}\,I_T(d), \tag{67}$$

where

$$I_T(d) = \int_{-\infty}^{\infty} \exp(-2x^2)\left[\frac{1+\text{erf}(x)}{2}\right]^{d-1}dx. \tag{68}$$

Note that for $d = 2$ and $d = 3$, we respectively have

$$I_T(2) = \frac{\pi}{2\sqrt{2}} \tag{69}$$

and

$$I_T(3) = \frac{1}{2\sqrt{2\pi}}\cos^{-1}(-\frac{1}{3}). \tag{70}$$

Substitution of these formulas into (67) recovers the results for $\bar{R}$ listed in Tables I and II for the equilateral triangle and tetrahedron, respectively. For large d, it is simple to show that

$$I_T(d) \sim \frac{2\pi\sqrt{\ln d}}{d^2}, \tag{71}$$

which implies

$$\bar{R} \sim \sqrt{\frac{\ln d}{d}}, \qquad d \to \infty. \tag{72}$$

We see that in the large-d limit, the radii of mean curvature for a regular hyperoctahedron and regular hypertetrahedron become identical.

The surface area and volume of a regular hypertetrahedron are given respectively by
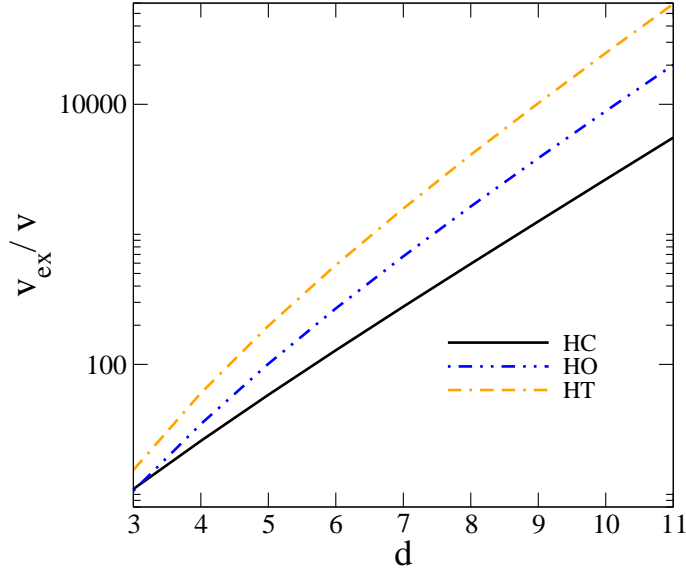
$$s = \frac{\sqrt{d}(d+1)}{2^{(d-1)/2}(d-1)!} \tag{73}$$

FIG. 3: (Color online) The dimensionless exclusion volume v_{ex}/v versus dimension d for the three convex regular polytopes: hypercube, hyperoctahedron and hypertetrahedron.

and

$$v = \frac{\sqrt{d+1}}{2^{d/2}d!}. \tag{74}$$

These relations combined with Eqs. (25) and (67) yield the exclusion volume to be given by

$$\frac{v_{\text{ex}}}{v} = 2 + \frac{d^{3/2}(d+1)^{3/2}\,\Gamma(\frac{d}{2})(2^{d-1}-1)}{\pi\Gamma(\frac{d-1}{2})}I_T(d). \tag{75}$$

In the large-d limit, this relation and (72) yield the asymptotic result

$$\frac{v_{\text{ex}}}{v} \sim \sqrt{2d\ln(d)}\,2^d, \qquad d \to \infty. \tag{76}$$

Among the three possible convex regular polytopes in high dimensions (hypercube, hyperoctahedron and hypertetrahedron), the hypertetrahedron has the largest dimensionless exclusion volume v_{ex}/v for any fixed dimension $d \geq 3$, while the hypercube has the smallest value. Figure 3 shows v_{ex}/v versus d for $3 \leq d \leq 11$ for the three convex regular polytopes.

D. Hyperplates

1. $(d-1)$-cube in $\mathbb{R}^d$

Consider a hyperplate in d-dimensional space that is a $(d-1)$-cube with side length a. The radius of mean curvature and exclusion volume of such a hyperplate are trivially obtained from special cases of relations (47) and (48). That is, setting $b = 0$ in (47) yields

$$\bar{R} = \frac{(d-1)\Gamma(1+\frac{d}{2})}{d\sqrt{\pi}\,\Gamma(\frac{d+1}{2})}\,a\,. \tag{77}$$

The corresponding exclusion volume is extracted from (48) by first multiplying both sides of the equation by the volume $v = a^{d-1}b$, and then setting $b = 0$, yielding

$$v_{\text{ex}} = \frac{4(d-1)(2^{d-1}-1)\Gamma(1+\frac{d}{2})}{d^2\sqrt{\pi}\,\Gamma(\frac{d+1}{2})}\,a^d, \tag{78}$$

which, not surprisingly, is smaller than the exclusion volume (43) for a d-cube in $\mathbb{R}^d$ at fixed d. Not surprisingly, in the high-d limit, formula (77) for the radius of mean curvature tends to the same asymptotic expression (42) for a d-cube in $\mathbb{R}^d$. This is not the case for the high-d limit of (78) for the exclusion volume, which is given by

$$v_{\text{ex}} \sim \sqrt{\frac{2}{d\pi}}\, 2^d\, a^d, \qquad d \to \infty, \tag{79}$$

and should be compared to (44), which grows faster as d increases.

Note that in the case $d = 3$, the formulas (77) and (78) give the same results reported in Table II for the instance of a square plate in $\mathbb{R}^3$. For $d = 2$, they also yield the relations (35) and (36) for the case of a randomly oriented line in $\mathbb{R}^2$.

2. $(d-1)$-sphere in $\mathbb{R}^d$

Consider a hyperplate in d-dimensional space that is a $(d-1)$-sphere of radius a. For such a hyperplate, $\bar{R}$ can be obtained from the corresponding relation (77) for a cubical hyperplate by multiplying the latter by the factor

$$\frac{\sqrt{\pi}\,\Gamma(\frac{d}{2})}{\Gamma(\frac{d+1}{2})},$$

which is the ratio of radius of mean curvature $\bar{R} = a$ of a $(d-1)$-sphere in $\mathbb{R}^{d-1}$ to that of the $(d-1)$-cube of side length a in $\mathbb{R}^{d-1}$, the latter of which is obtained by using (41). Thus, the radius of mean of curvature for a $(d-1)$-sphere of radius in $\mathbb{R}^d$ is given by

$$\bar{R} = \frac{(d-1)\,\Gamma(\frac{d}{2})^2}{2\,\Gamma(\frac{d+1}{2})^2}\, a\,. \tag{80}$$

To illustrate the fact that this simple mapping is equivalent to the explicit calculation of $\bar{R}$ for a $(d-1)$-sphere, we carry out such a computation in Appendix A for a 3-sphere in $\mathbb{R}^4$. Using the fact that the surface area of a $(d-1)$-sphere in $\mathbb{R}^d$ is $s = 2v_s(d-1; a)$, where $v_s(d; a)$ is given by (18), we obtain the d-dimensional exclusion volume to be

$$v_{\text{ex}} = \frac{2(d-1)(2^{d-1}-1)\pi^{(d-1)/2}\Gamma(\frac{d}{2})^2}{d\,\Gamma(\frac{d+1}{2})^3}\, a^d < \frac{2^d \pi^{d/2}}{\Gamma(1+d/2)}\, a^d, \tag{81}$$

where the upper bound is the exclusion volume of a d-sphere in $\mathbb{R}^d$ [7]. Not surprisingly, in the high-d limit, formula (80) for the radius of mean curvature tends to the radius a. In this asymptotic limit, relation (81) becomes

$$v_{\text{ex}} \sim \frac{2^{3/2}}{d\,\sqrt{\pi}} \left(\frac{2\pi\exp(1)}{d}\right)^{d/2} 2^d\, a^d < \frac{1}{\sqrt{d\pi}} \left(\frac{2\pi\exp(1)}{d}\right)^{d/2} 2^d\, a^d. \tag{82}$$

Observe that in the case $d = 3$, the formulas (80) and (81) give the same results reported in Table II for the instance of a circular plate in $\mathbb{R}^3$. For $d = 2$, they also yield the relations (35) and (36) for the case of a randomly oriented line in $\mathbb{R}^2$.

V. CONJECTURE FOR THE MAXIMUM-THRESHOLD HYPERPARTICLE SHAPE AMONG ALL CONVEX BODIES IN $\mathbb{R}^d$

Recall that the dimensionless exclusion volume v_{ex}/v, among all convex bodies in $\mathbb{R}^d$ with a nonzero d-dimensional volume, is minimized for hyperspheres [see Sec. II B] and its threshold η_c exactly tends to $v/v_{\text{ex}} = 2^{-d}$ in the high-dimensional limit [cf. (5)]. These properties together with the principle that low-d percolation properties encode high-d information [7], leads us to the following conjecture:

Conjecture: The percolation threshold η_c among all systems of overlapping randomly oriented convex hyperparticles in $\mathbb{R}^d$ having nonzero volume is maximized by that for hyperspheres, i.e.,

$$(\eta_c)_S \geq \eta_c, \tag{83}$$

where $(\eta_c)_S$ is the threshold of overlapping hyperspheres.

We note that similar reasoning leading to the aforementioned conjecture (83) for convex hyperparticles of nonzero volume also suggests that the dimensionless exclusion volume $v_{\text{ex}}/v_{\text{eff}}$ associated with a convex $(d-1)$-dimensional hyperplate in $\mathbb{R}^d$ is minimized by the $(d-1)$-dimensional hypersphere, which consequently would have the highest percolation threshold among all convex hyperplates. Recall that v_{eff} the effective d-dimensional volume associated with the zero-volume hyperplate of interest, defined by (12).

VI. ACCURATE SCALING RELATION FOR THE PERCOLATION THRESHOLD OF OVERLAPPING CONVEX HYPERPARTICLES

Recall that lower bound (7) on the threshold η_c of overlapping convex hyperparticles of general shapes with nonzero volumes and a specified orientational distribution is determined by the dimensionless exclusion volume v_{ex}/v, which also provides the exact high-d asymptotic limit [cf. (10)]. A special case of this lower bound is the inequality (31), which is valid for hyperspheres as well as aligned centrally symmetric particles for which $v_{\text{ex}}/v = 2^d$.

Guided by the aforementioned high-dimensional behavior of η_c, conjecture (83) for hyperspheres, and the functional form of the lower bounds (3) and (7), we propose the following scaling law for the threshold η_c of overlapping nonspherical convex hyperparticles of arbitrary shape and orientational distribution having nonzero volumes for any dimension d:

$$
\begin{aligned}
\eta_c &\approx \left(\frac{v_{\text{ex}}}{v}\right)_S \left(\frac{v}{v_{\text{ex}}}\right)(\eta_c)_S \\
&= 2^d \left(\frac{v}{v_{\text{ex}}}\right)(\eta_c)_S,
\end{aligned}
\tag{84}
$$

where $(\eta_c)_S$ and $(v_{\text{ex}}/v)_S = 2^d$ are the percolation threshold and dimensionless exclusion volume, respectively, for hyperspheres in dimension d. Thus, given the percolation threshold for the *reference system* of hyperspheres $(\eta_c)_S$ and the dimensionless exclusion volume v_{ex}/v for some general nonspherical convex hyperparticle shape with a specified orientational distribution, one can estimate the threshold η_c of such a system of overlapping hyperparticles across dimensions via the scaling relation (84). Note that this scaling relation becomes exact in the high-d limit. In the next section, we will show that this scaling relation provides reasonably accurate estimates of η_c in low dimensions and, hence, must become increasingly accurate as d becomes large. This is yet another manifestation of the principle that low-dimensional percolation properties encode high-dimensional information [7].

It is noteworthy that the scaling relation (84) not only provides a good approximation for the threshold η_c of overlapping nonspherical hyperparticles, it yields an upper bound on η_c, and hence a relatively tight one. Explicitly, we have the following d-dimensional inequality:

$$
\eta_c \geq 2^d \left(\frac{v}{v_{\text{ex}}}\right)(\eta_c)_S.
\tag{85}
$$

This bounding property is a consequence of an observation made in Ref. 7, namely, that, at fixed d, the lower bound (7) on $(\eta_c)_S$ for overlapping hyperspheres converges more slowly to its exact asymptotic value of 2^{-d} than does the lower bound (7) for nonspherical hyperparticles with a specified orientational distribution. It then immediately follows from the functional form of (84) that it bounds η_c for nonspherical hyperparticles from above and converges to the exact asymptotic value of v/v_{ex} in the large-d limit [cf. (10)].

For a zero-volume convex $(d-1)$-dimensional hyperplate in $\mathbb{R}^d$, it is more appropriate to choose the *reference system* to be $(d-1)$-dimensional hyperspheres of characteristic radius r, yielding the scaling relation for the threshold for some other hyperplate shape to be

$$
\begin{aligned}
\eta_c &\approx \left(\frac{v_{\text{ex}}}{v_{\text{eff}}}\right)_{SHP} \left(\frac{v}{v_{\text{ex}}}\right)(\eta_c)_{SHP} \\
&= 2^d \left(\frac{v_{\text{eff}}}{v_{\text{ex}}}\right)(\eta_c)_{SHP}.
\end{aligned}
\tag{86}
$$

Here $(\eta_c)_{SHP}$ is the percolation threshold for a $(d-1)$-dimensional hypersphere and v_{eff} is its effective volume, as defined by relation (12).

We will test these scaling laws and bounds for a variety of hyperparticle shapes across various dimensions using the exclusion volumes presented in Secs. III and IV and comparing these results to available numerically-determined threshold estimates, including those values that we have obtained below for the Platonic solids.

VII. APPLICATION OF THE SCALING RELATION AND BOUNDS

Here, we apply the lower bound (7) and scaling relation (84) to estimate η_c for a wide class of randomly oriented overlapping nonspherical hyperparticles in $\mathbb{R}^d$, including, among other shapes, various polygons for $d = 2$, Platonic solids, spherocylinders, parallepipeds and zero-volume plates for $d = 3$ and their appropriate generalizations for $d \geq 4$, when possible. We test these estimates against available numerical results for η_c in $\mathbb{R}^2$ and $\mathbb{R}^3$, including those obtained here for Platonic solids using the rescaled-particle method [8].

A. Two Dimensions

TABLE IV: Percolation threshold η_c of certain overlapping convex particles K with random orientations in $\mathbb{R}^2$, estimated using Eq. (84) and the associated threshold values η_c^* for squares [25, 26] and ellipses [27–29] obtained from previous numerical simulations. The threshold of overlapping circles [30, 31] is also given, which is employed to compute the estimates.

K	η_c^*	η_c
Circle	1.1281	
Square	0.9822	0.9925
Ellipse $b = 2a$	0.76	1.107
Ellipse $b = 5a$	0.607	0.7174
Ellipse $b = 10a$	0.358	0.4402
Ellipse $b = 100a$	0.0426	0.0543
Octagon		1.0980
Hexagon		1.0730
Pentagon		1.0463
Equilateral Triangle		0.8501
Rectangle $a_2 = 2a_1$		0.9275
Spherocylinder $h = 2a$		1.0357

Table IV gives the percolation threshold η_c estimated using the scaling relation (84) for a variety of randomly oriented overlapping particles in $\mathbb{R}^2$. In the cases of squares and ellipses with different aspect ratios, the associated threshold value η_c^* obtained from numerical simulations [25–29] are also given in the table. Clearly, for most of randomly oriented nonspherical particles, the scaling relation not only bounds η_c from above, consistent with inequality (85), the bounds are relatively tight. Since the scaling relation already provides a good estimate for $d = 2$, it will increasingly become accurate as d increases for reasons discussed in Sec. VI. We will see below that this is indeed the case for $d = 3$.

B. Three Dimensions

1. Nonzero-Volume Convex Bodies

The percolation thresholds for randomly oriented overlapping Platonic solids (i.e., tetrahedron, octahedron, dodec-ahedron, icosahedron and cube) are estimated using a recently developed rescaled-particle method. Implementation of this algorithm for the Platonic solids is described in Appendix B of this paper. In Ref. 8, the rescaled-particle method was applied to obtain accurate estimates of η_c for overlapping hyperspheres and oriented hypercubes.

Table V lists the numerical estimates of η_c, the associated lower-bound values η_L given by (7), and the numerical values of the dimensionless exclusion volumes for these polyhedra v_{ex}/v (whose analytical expressions are given in Table II). Observe that the tetrahedron and icosahedron possess the smallest and largest percolation thresholds, respectively, among the Platonic solids, which is confirmed in Table V. As discussed above, this implies that the the tetrahedron and icosahedron possess the largest and smallest dimensionless exclusion volumes, respectively, among the Platonic solids. We note that our estimate of η_c for randomly oriented overlapping cubes is consistent with that reported in Ref. 25, i.e., $\eta_c = 0.2444 \pm 0.0003$, which verifies the accuracy of our approach for estimating η_c. The number within the parentheses represents the error in the last digit. These results will be employed below to verify the accuracy of the general scaling relation (84) for estimating η_c of nonspherical convex hyperparticles across dimensions, since the scaling relation becomes increasingly accurate as d increases, as discussed in Sec. VI.

TABLE V: Numerically estimated percolation threshold η_c of randomly oriented overlapping Platonic solids and the associated lower bound value η_L given by (7). The numerical values of the dimensionless exclusion volumes of these polyhedra v_{ex}/v, whose analytical expressions are given in Table II, are also included

K	v_{ex}/v	η_L	η_c
Tetrahedron	15.40743	0.06493	0.1701±0.0007
Cube	11	0.09090	0.2443±0.0005
Octahedron	10.63797	0.09398	0.2514±0.0006
Dodecahedron	9.12101	0.1096	0.2949±0.0005
Icosahedron	8.91526	0.1126	0.3030±0.0005

TABLE VI: Percolation threshold η_c of certain overlapping convex particles K with random orientations in $\mathbb{R}^3$, estimated using Eq. (84) and the associated threshold values η_c^* for regular polyhedra (obtained from our numerical simulations) and spheroids [29]. The threshold of overlapping spheres [8, 32] is also given, which is employed to compute the estimates.

K	η_c^*	η_c
Sphere	0.3418	
Tetrahedron	0.1701	0.1774
Icosahedron	0.3030	0.3079
Decahedron	0.2949	0.2998
Octahedron	0.2514	0.2578
Cube	0.2443	0.2485
Oblate spheroid $a = c = 100b$	0.01255	0.01154
Oblate spheroid $a = c = 10b$	0.1118	0.104
Oblate spheroid $a = c = 2b$	0.3050	0.3022
Prolate spheroid $a = c = b/2$	0.3035	0.3022
Prolate spheroid $a = c = b/10$	0.09105	0.104
Prolate spheroid $a = c = b/100$	0.006973	0.01154
Parallelpiped $a_2 = a_3 = 2a_1$		0.2278
Cylinder $h = 2a$		0.4669
Spherocylinder $h = 2a$		0.2972

Estimates of the percolation threshold η_c using the scaling relation (84) for a variety of randomly oriented overlapping particles in $\mathbb{R}^3$ are presented in Table VI. These predictions are compared to numerically determined threshold values. We see that for most of the randomly oriented nonspherical particles, the scaling relation (84), which is also an upper bound [cf. (85)], only slightly overestimates η_c compared with the numerical results. For oblate spheroids and prolate spheroid of aspect ratio 2, the scaling relation slightly underestimates η_c compared to the numerical values, implying that the numerical results are overestimates of the actual threshold for these systems, i.e., the numerical estimates in these instances violate the upper bound (85). These three-dimensional results show that scaling relation (84) for η_c improves in accuracy over the two-dimensional results reported in Table IV.

2. Zero-Volume Convex Plates

Table VII lists the percolation threshold η_c obtained from the scaling relation (84) and numerical simulations for a variety of randomly oriented overlapping zero-volume two-dimensional plates in $\mathbb{R}^3$. As per relation (12), the effective volume of these plates is chosen to be the volume of a sphere whose radius r is a characteristic length scale of the associated plate. In particular, for circular disks, r is chosen to be radius of the disk. For noncircular plates, r is the radius of a disk whose area is the same as that of the noncircular plate of interest [33]. Importantly, the reference system for the scaling relation is randomly oriented overlapping circular disks, which is also given in the table. Again, the scaling relation (84) only slightly overestimates η_c in the case of the triangular and elliptical plates. For square plates, the scaling relation slightly underestimates η_c, suggesting that the numerical results overestimate the actual percolation threshold for this system.

TABLE VII: Percolation threshold η_c of certain overlapping convex plates K with random orientations in $\mathbb{R}^3$, estimated using Eq. (84). The associated threshold values η_c^* obtained from previous numerical simulations [33] are also given if available. The threshold of randomly oriented overlapping circular disks is also given, which is employed to compute the estimates. The numerical values of η_c^* listed here are given up to the number of significant figures reported in Ref. 33.

K	η_c^*	η_c
Circular disk	0.9614	
Square plate	0.8647	0.8520
Triangular plate	0.7295	0.7475
Elliptical plate $b = 3a$	0.735	0.7469
Rectangular plate $a_2 = 2a_1$		1.0987

C. Dimensions Four Through Eleven

1. Nonzero-Volume Convex Bodies

In Table VIII, we provide the percolation threshold η_c of d-dimensional overlapping hyperspheres and oriented hypercubes for $4 \leq d \leq 11$ obtained previously via the rescaled-particle method [8]. As expected, the threshold values for the two systems approach each other as d increases and become identical in the limit $d \to \infty$, i.e., $\eta_c \to 1/2^d$ [7]. The results for hyperspheres will be used to estimate η_c for the hyperparticles discussed in Sec. IV.

TABLE VIII: Numerical estimates of the percolation threshold η_c of d-dimensional overlapping hyperspheres and oriented hypercubes for $4 \leq d \leq 11$ reported in Ref. 8. The threshold values for the two systems, given up to the number of significant figures reported in Ref. 8, approach each other as d increases and become identical in the asymptotic limit $d \to \infty$, i.e., $\eta_c \to 1/2^d$ [7].

Dimension	Hypersphere	Hypercube
$d=4$	0.1304	0.1201
$d=5$	0.05443	0.05024
$d=6$	0.02339	0.02104
$d=7$	0.01051	0.01004
$d=8$	0.004904	0.004498
$d=9$	0.002353	0.002166
$d=10$	0.001138	0.001058
$d=11$	0.0005530	0.0005160

TABLE IX: Percolation threshold η_c of certain d-dimensional randomly overlapping hyperparticles estimated using Eq. (84) for $4 \leq d \leq 11$, including hypercubes (HC), hyperrectangular parallelpiped (HRP) of aspect ratio 2 (i.e., $a_1 = 2a$ and $a_i = a$ for $i = 2, \ldots, d$), hyperspherocylinder (HSC) of aspect ratio 2 (i.e., $h = 2a$), hyperoctahedra (HO) and hypertetrahedra (HT).

Dimension	HC	HRP	HSC	HO	HT
$d = 4$	8.097×10^{-2}	7.452×10^{-2}	1.109×10^{-1}	6.009×10^{-2}	3.471×10^{-2}
$d = 5$	2.990×10^{-2}	2.775×10^{-2}	4.599×10^{-2}	1.724×10^{-2}	8.808×10^{-3}
$d = 6$	1.167×10^{-2}	1.092×10^{-2}	1.975×10^{-2}	5.560×10^{-3}	2.580×10^{-3}
$d = 7$	4.846×10^{-3}	4.568×10^{-3}	8.899×10^{-3}	1.986×10^{-3}	8.518×10^{-4}
$d = 8$	2.116×10^{-3}	2.006×10^{-3}	4.167×10^{-3}	7.659×10^{-4}	3.071×10^{-4}
$d = 9$	9.584×10^{-4}	9.133×10^{-4}	2.007×10^{-3}	3.129×10^{-4}	1.180×10^{-4}
$d = 10$	4.404×10^{-4}	4.214×10^{-4}	9.746×10^{-4}	1.314×10^{-4}	4.696×10^{-5}
$d = 11$	2.044×10^{-4}	1.963×10^{-4}	4.754×10^{-4}	5.632×10^{-5}	1.917×10^{-5}

To our knowledge, no numerical estimates of η_c are available for hyperparticles for $d \geq 4$. Simulations are difficult to carry out due to the increasing complexity in accurately detecting particle overlap as d increases. Given the accuracy of the scaling relation (84), verified by numerical results in $\mathbb{R}^2$ and $\mathbb{R}^3$, we now apply it to estimate η_c for the d-dimensional randomly oriented overlapping hyperparticles discussed in Sec. IV, where it should provide even
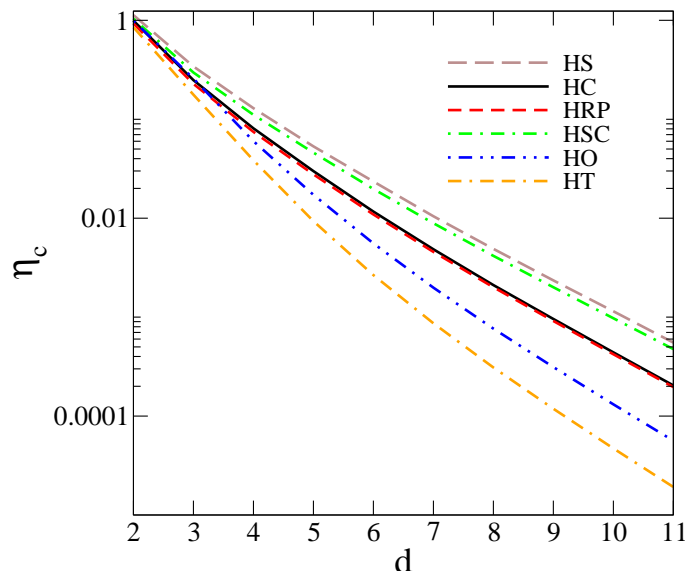
FIG. 4: (Color online) Percolation threshold η_c versus dimension d as obtained from scaling relation (84) for randomly oriented overlapping nonspherical hyperparticles, including hypercubes (HC), hyperrectangular parallelpipeds (HRP) of aspect ratio 2 (i.e., $a_1 = 2a$ and $a_i = a$ for $i = 2, \ldots, d$), hyperspherocylinder (HSC) of aspect ratio 2 (i.e., $h = 2a$), hyperoctahedra (HO) and hypertetrahedra (HT). Values of η_c for hyperspheres (HS) [8] are also shown for purposes of comparison.

better predictions. Table IX summarizes threshold values for various hyperparticles for $4 \leq d \leq 11$ using (84)) and the thresholds for hyperspheres listed in Table VIII. As expected, η_c for randomly oriented hypercubes is lower than that for oriented hypercubes in the corresponding dimensions.

The threshold η_c versus d for the systems listed in Table IX is plotted Fig. 4. As expected, threshold values of nonspherical hyperparticles are always below that of hyperspheres for any fixed d. For hyperspherocylinders of aspect ratio 2 (i.e., $h = 2a$), the associated η_c is only slightly below the hypersphere value in the corresponding dimensions. Similarly, for hyperrectangular parallelpipeds of aspect ratio 2 (i.e., $a_1 = 2a$ and $a_i = a$ for $i = 2, \ldots, d$), η_c is only slightly below the hypercube value in the corresponding dimensions.

To obtain excellent estimates of η_c for nonspherical hyperparticles for $d \geq 12$, one can use the scaling relation (84) together with highly accurate analytical expressions for hyperspheres in high dimensions given in Ref. 7; see, e.g., Eqs. (86) and (119) in that paper.

2. Zero-Volume Convex Hyperplates

The left panel of Fig. 5 shows the dimensionless exclusion volume $v_{\mathrm{ex}}/v_{\mathrm{eff}}$ versus d for spherical and cubical hyperplates. Recall that the effective volume v_{eff} of a hyperplate [i.e., a $(d-1)$-dimensional object in $\mathbb{R}^d$] is chosen to be the volume of a d-sphere with radius r that is a characteristic length scale of the hyperplate. For spherical hyperplates, r is chosen to be radius of the hyperplate. For cubical hyperplates, r is the radius of a $(d-1)$-sphere whose $(d-1)$-dimensional volume (or d-dimensional area) is the same as that of the cubical hyperplate. Clearly, $v_{\mathrm{ex}}/v_{\mathrm{eff}}$ for spherical hyperplates is smaller than that for cubical hyperplates in all dimensions $d \geq 3$. Lower bounds on η_c for spherical and cubical hyperplates, as obtained from inequality (13), are shown in the right panel of Fig. 5. As expected, the lower bound for spherical hyperplates is always greater than that for cubical hyperplates in all dimensions $d \geq 3$.

VIII. CONCLUSIONS AND DISCUSSION

We have exploited the principle that low-dimensional continuum percolation behavior encodes high-dimensional information, recent analytical results on the percolation threshold η_c of continuum percolation models [7] and conjecture (83) to formulate the scaling relation (84) for η_c that is applicable to a wide variety of overlapping nonspherical hyperparticles with random orientations for any dimension d. This scaling relation, which is also an upper bound on η_c,
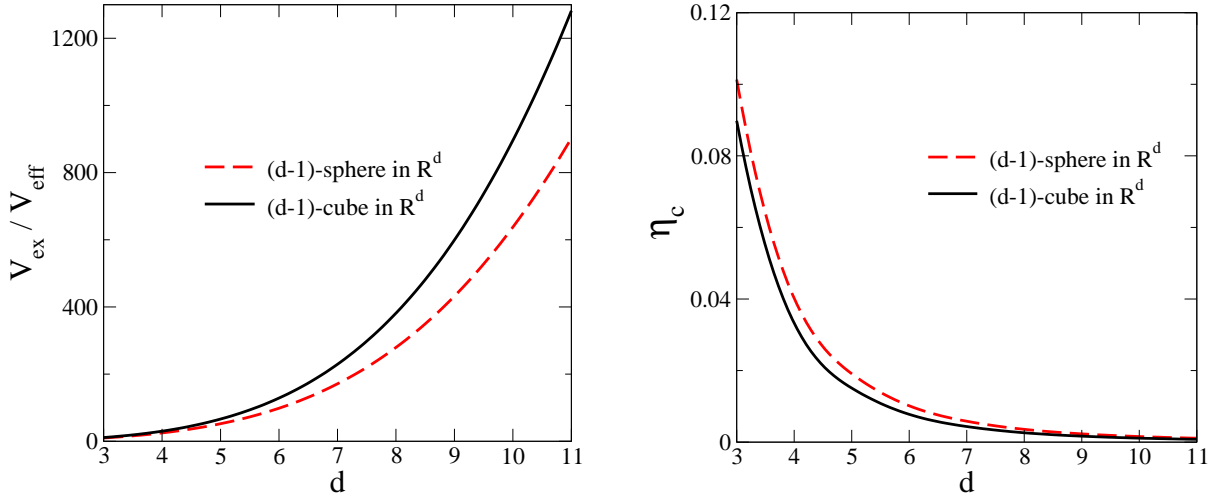
FIG. 5: (Color online) Left panel: Dimensionless exclusion volume v_{ex}/v_{eff} versus dimension d for spherical and cubical hyperplates. Right panel: Lower bounds on the percolation threshold η_c versus dimension d for spherical and cubical hyperplates.
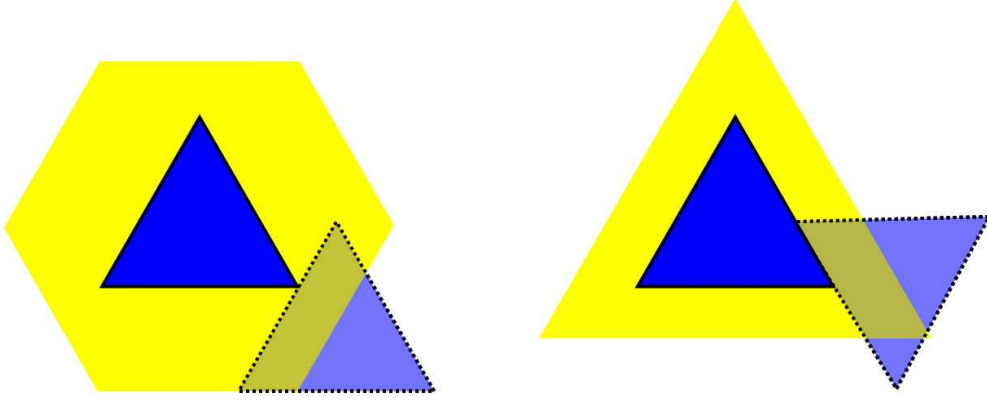

FIG. 6: (Color online) Exclusion region associated with equilateral triangles with volume v with specific relative particle orientations in $\mathbb{R}^2$. Left panel: Triangles are perfectly aligned. The associated exclusion region is a regular hexagon (yellow region) whose edge length is the same as that of the triangle, resulting in $v_{ex}/v = 6$. Right panel: Triangles are oriented in such a way that one can be mapped to another by a center inversion operation. Here two particles always form edge-to-edge contacts. The associated exclusion region is a larger equilateral triangle (yellow region) whose edge length is twice that of the original triangle, resulting in $v_{ex}/v = 4$.

depends on the d-dimensional exclusion volume v_{ex} associated with a hyperparticles and was determined analytically for, among other shapes, various polygons for $d = 2$, Platonic solids, spherocylinders, parallelepipeds and zero-volume plates for $d = 3$ and their appropriate generalizations for $d \geq 4$. The scaling relation already provides a good estimate of η_c for $d = 2$, becomes increasingly accurate as d increases, and becomes exact in the high-d limit. The new estimates of the percolation thresholds obtained from the scaling relation could have implications for a variety of chemical and physical phenomena involving clustering and percolation behavior described in the Introduction. It will be interesting to see if our conjecture that overlapping hyperspheres provide the highest threshold among all overlapping systems of convex hyperparticle shapes for any d [cf. (83)] can be proved.

The exclusion volume v_{ex} also has physical importance in other fields besides percolation, such as granular materials, packing problems, and phase transitions in condensed-matter systems. For example, v_{ex} plays a critical role in the well-known isotropic-nematic transition in hard-rod systems studied by Onsager [34]. Thus, our comprehensive study of v_{ex} could also deepen our understanding of a variety of other problems in condensed matter physics. The relevance of v_{ex} to packing problems is briefly discussed below.

Although the main focus of this paper concerned the percolation threshold of *randomly* oriented overlapping hyper-particles, the bound (7) and the scaling relation (84) are also valid for overlapping particles with specific orientational distributions when the general relation (9) for the exclusion volume v_{ex} is used. To illustrate this point, we appeal to two-dimensional examples depicted in Fig. 6, which shows the exclusion regions associated with equilateral triangles in $\mathbb{R}^2$ with two different particle orientations: fully aligned and edge-to-edge . Equilateral triangles are not centrally symmetric and so its exclusion volume v_{ex} is minimized for the edge-to-edge configuration (i.e., $v_{ex}/v = 4$) and max-imized when the particles are aligned (i.e., $v_{ex}/v = 6$). The exclusion volume for other relative orientations must be between these two extremal values. For example, we see from Table 22, $v_{ex}/v = 5.30797\ldots$ for randomly oriented equilateral triangles. Thus, in order of increasing values of v_{ex}/v for these three examples, we have the lower bounds $\eta_c \geq 0.25$ (edge-to-edge) , $\eta_c \geq 0.188395\ldots$ (random), and $\eta_c \geq 0.166666\ldots$ (aligned), respectively, as predicted by (7). The actual threshold trends for these three cases should follow those given by these bounds, as does the corresponding predictions of the scaling relation: $\eta_c \approx 1.1281$, $\eta_c \approx 0.8501$, and $\eta_c \approx 0.7520$.

It is noteworthy that the magnitude of the dimensionless exclusion volume v_{ex}/v of a convex body with some specified orientation distribution is closely related to how densely such *nonoverlapping* objects can be packed in space [35]. In particular, the ratio v_{ex}/v for a centrally symmetric convex hyperparticle is minimized when the bodies are aligned [7]. For noncentrally symmetric convex shapes, nonaligned orientations result in a smaller value of v_{ex}/v relative to that of the aligned case (see Fig. 6). These exclusion-volume properties of centrally and noncentrally symmetric bodies play a major role in recently proposed organizing principles concerning optimal (i.e., maximally dense) packings of both hard convex and hard concave particles in $\mathbb{R}^3$ [35]. Among other results, it was conjectured that the optimal packing of a centrally symmetric particle is achieved by the associated optimal Bravais-lattice packing in which all the particles are aligned (e.g., superballs [36]); while the optimal packing of a particle without central symmetry (e.g., truncated tetrahedra [37]) is generally given by a non-Bravais-lattice packing in which the particles have different nonaligned orientations.

In the Introduction, we discussed the duality between the equilibrium hard-hyperparticle fluid system and the continuum percolation model of overlapping hyperparticles of the same shape. A consequence of this duality relation and the so-called decorrelation principle for disordered hard-hyperparticle packings [38, 39] led to the result that the large-d percolation threshold η_c of overlapping hyperparticles is directly related to the large-d *freezing-point* density (onset of disorder-order phase transition) of corresponding equilibrium hard-hyperparticle models [7]. In a future work, we shall explore this duality relationship to predict the onset of phase transitions in hard-hyperparticle fluids across dimensions. Finally, we will show elsewhere that the lower-order Padé] approximants studied in Ref. 7 lead also to bounds on the percolation threshold for lattice-percolation models in arbitrary dimension.

Appendix A: Explicit Calculation of the Mean Width $\bar{w}$ of A Three-Dimensional Spherical Hyperplate in $\mathbb{R}^4$

In Sec. II, we presented an explicit method to calculate the mean width $\bar{w} = 2\bar{R}$ of a convex body in $\mathbb{R}^d$. Recall that the width $w(\mathbf{n})$ of a convex body is the smallest distance between two impenetrable parallel $(d-1)-$dimensional hyperplanes contacting the boundaries of the body, where $\mathbf{n}$ is a unit vector orthogonal to the hyperplanes. The mean width $\bar{w}$ is the average of the width $w(\mathbf{n})$ of the body such that $\mathbf{n}$ is uniformly distributed over the unit sphere $S^{d-1} \in \mathbb{R}^d$. Here, we employ this method to obtain $\bar{w}$ of a three-dimensional spherical hyperplate (i.e., 3-sphere) of radius a in $\mathbb{R}^4$.

Due to the rotational symmetry of the 3-sphere, its orientation in $\mathbb{R}^4$ is specified by a unit vector $\mathbf{u}$, which is analogous to the case of a circular disk in $\mathbb{R}^3$; see Table III. The width $w(\mathbf{n})$ of the 3-sphere is given by

$$w(\mathbf{n}) = 2a\sqrt{1- <\mathbf{u}, \mathbf{n}>^2} = 2a\sin\theta, \tag{A-1}$$

where $<\mathbf{x}, \mathbf{y}>$ is the inner product of two vectors $\mathbf{x}$ and $\mathbf{y}$, and θ is the angle between $\mathbf{u}$ and $\mathbf{n}$. Therefore, the mean width is given by

$$\bar{w} = \frac{1}{\Omega} \int 2a\sin\theta \, dS^3 = \frac{1}{\Omega} \int_0^{2\pi} \int_0^\pi \int_0^\pi 2a\sin^2\theta \sin\phi \, d\theta d\phi d\psi, \tag{A-2}$$

where

$$\Omega = \int dS^3 = \int_0^{2\pi} \int_0^{\pi} \int_0^{\pi} \sin\theta \sin\phi \ d\theta d\phi d\psi = 2\pi^2, \tag{A-3}$$

is the 4-dimensional solid angle. Carrying out the integration in Eq. (A-2) yields the mean width $\bar{w}$ of 3-sphere in $\mathbb{R}^4$, i.e.,

$$\bar{w} = \frac{1}{2\pi^2} \times \frac{16\pi a}{3} = \frac{8a}{3\pi}. \tag{A-4}$$

Appendix B: Rescaled-Particle Method for Estimating η_c of Randomly Oriented Overlapping Platonic Solids

In Ref. 8, we devised a highly efficient rescaled-particle method to estimate η_c for d-dimensional hyperspheres and oriented hypercubes, utilizing the tightest lower bound on η_c, i.e., the pole of the [2, 1] Padé approximant of the mean cluster size S, obtained in Ref. 7; see Eq. (119) in that paper. The basic idea behind this method is to begin with static configurations of overlapping particles at a reduced density η_0 that is taken to be the best lower-bound value and then to increase η by rescaling the particle sizes until a system-spanning cluster forms. This algorithm enables one to accurately estimate η_c in a computationally efficient manner, even in high dimensions [8]. Here, we adapt the method to investigate percolation properties of randomly oriented overlapping Platonic solids, including tetrahedra, icosahedra, dodecahedra, octahedra, and cubes in $\mathbb{R}^3$. Except for overlapping cubes, whose percolation properties have been well-studied, the percolation thresholds for the other polyhedra have heretofore not been investigated.

Initially, a Poisson distribution of a large number of points in the periodic simulation domain is generated. Each point is then taken to be the centroid of a polyhedron with a random orientation and a characteristic length ℓ_0 (e.g., the diameter of the associated circumsphere). The initial value of ℓ_0 is chosen so that the initial reduced density η_0 of the system equals the lower-bound value given by (7). For each polyhedron i, a near-neighbor list (NNL) is obtained that contains the centroids of the polyhedra j whose distance D_{ij} to particle i is smaller than $\gamma\ell_0$ ($\gamma > 1$). The value of γ generally depends on the specific polyhedron of interest. A good choice for γ is a value that yields a NNL list that only contains polyhedra that overlap at the threshold. In our simulations, we used $\gamma \in [1.25, 1.5]$, depending on the asphericity of the shapes [40, 41]. Then the sizes of the polyhedra are slowly and uniformly increased by increasing ℓ_0, leading to an increase of the reduced density by an incrementally small amount $\delta\eta$. After each system rescaling, the polyhedra in the NNL are checked for overlap using the separation axis theorem [41] and the largest cluster is identified. This process is repeated until a system-spanning cluster forms.

Since static particle configurations and a predetermined NNL are used, the complexity of cluster identification is significantly reduced. Because initial configurations with relatively high reduced density values (i.e., the lower bound values) are used, the amount of rescaling before the system percolates is much smaller than that from an initial low-density configuration. Furthermore, the reduced density η can be incremented by a small amount $\delta\eta$ as η_c is approached, leading to a more accurate estimate of the percolation threshold.

For each of the Platonic solids, we use several distinctly different system sizes, i.e., $N = 5000, 10000, 50000, 100000$, and for each system size, we generate 500 independent realizations of the overlapping polyhedra. The results are extrapolated by spline fitting the finite-system-size data in a log-log plot to obtain the infinite-system-size estimate of η_c.

[1] R. Zallen, *The Physics of Amorphous Solids* (Wiley, New York, 1983).
[2] C. J. Brinker and G. W. Scherer, *Sol-Gel Science: The Physics and Chemistry of Sol-Gel Processing* (Academic, New York, 1990).
[3] D. Stauffer and A. Aharony, *Introduction to Percolation Theory* (Taylor & Francis, London, 1992).
[4] M. Sahimi, Applications of Percolation Theory (Taylor and Francis, London, 1994).
[5] S. Torquato, Random Heterogeneous Materials: Microstructure and Macroscopic Properties (Springer-Verlag, New York, 2002).
[6] V. Myroshnychenko and C. Brosseau, J. Appl. Phys. **103**, 084112 (2008); S. El Bouazzaoui, A. Droussi, M. E. Achour, and C. Brosseau, J. Appl. Phys. **106**, 104107 (2009).
[7] S. Torquato, J. Chem. Phys. **136**, 054106 (2012).
[8] S. Torquato and Y. Jiao, J. Chem. Phys. **137**, 074106 (2012).
[9] Note that the volume of a hyperparticle was denoted by v_1 in Ref. 7. In the present paper, we drop the subscript 1, and simply denote this quantity by v.
[10] For equilibrium hard-particle systems, the total correlation function $h(r; \eta)$ generally takes on both negative and positive values depending on the values of the radial distance r and reduced density η. One can think of the duality relation (1) as the mapping that is required to convert a correlation function for a hard-particle system to a non-negative pair connectedness function (bounded from above by unity) for the corresponding overlapping particle system.
[11] A hyperparticle is centrally symmetric if its centroid is a point of inversion symmetry.
[12] Roughly speaking, the exclusion volume associated with a particle is the volume excluded to the centroid of another particle under the condition that the particles are impenetrable to one another. Thus, when a particle centroid is inside another particle's exclusion volume, the particles necessarily overlap one another. The reader is referred to Ref. 7 for additional details.
[13] S. Torquato, J. Stat. Phys. **45**, 843 (1986).
[14] C. E. Zachary and S. Torquato, Phys. Rev. E **84**, 056102 (2011).
[15] Balberg et al. [16] have suggested that the mean number of overlaps per particle at the threshold $\mathcal{N}_c$ is an approximant invariant for overlapping convex particles of general shape in two and three dimensions. Simulations have shown this not to be an invariant in these low dimensions. However, the asymptotic result (11) reveals that $\mathcal{N}_c$ is an invariant, with value unity, in the high-dimensional limit, regardless of the shape of the convex particle.
[16] I. Balberg, C. H. Anderson, S. Alexander, and N. Wagner, Phys. Rev. B **30**, 3933 (1984).
[17] D. Stoyan, W. S. Kendall, and J. Mecke, *Stochastic Geometry and Its Applications*, 2nd ed. (Wiley, New York, 1995).
[18] T. Boublík, Mol. Phys. **29**, 421 (1975).
[19] T. Kihara, Rev. Mod. Phys. **25**, 831 (1953).
[20] R. Schneider *Convex Bodies: The Brunn-Minkowski Theory* (Cambridge University Press, Cambridge, 1993).
[21] H. S. M. Coxeter, *Regular Polytopes* (Dover, New York, 1973).
[22] H. Hadwiger, Math. Annalen **239**, 271 (1979).
[23] U. Betke and M. Henk, Monatsh. Math. **115**, 27 (1993).
[24] M. Henk, J. Richter-Gebert, and G. M. Ziegler, in *Handbook of Discrete and Computational Geometry* (CRC Press, New York, 1997).
[25] D. R. Baker, G. Paul, S. Sreenivasan, and H. E. Stanley, Phys. Rev. E **66**, 046136 (2002).
[26] S. Mertens and C. Moore, arXiv.1209.4936 (2012).
[27] W. Xia and M. F. Thorpe, Phys. Rev. A **38**, 2650 (1988).
[28] Y. B. Yi and A. M. Sastry, Proc. R. Soc. Lond. A **460**, 2353 (2007).
[29] E. J. Garboczi, K. A. Snyder, J. F. Douglas, and M. F. Thorpe, Phys. Rev. E **52**, 819 (1995).
[30] J. Quintanilla, S. Torquato and R. M. Ziff, J. Phys. A: Math. Gen. **33**, L399 (2000).
[31] J. Quintanilla and R. M. Ziff, Phys. Rev. E **76**, 051115 (2007).
[32] C. D. Lorenz and R. M. Ziff, J. Chem. Phys. **114**, 3659 (2000).
[33] Y. B. Yi and E. Tawerghi, Phys. Rev. E **79**, 041134 (2009).
[34] L. Onsager, Phys. Rev. **65**, 117 (1944).
[35] S. Torquato and Y. Jiao, Phys. Rev. E **86**, 011102 (2012).
[36] Y. Jiao, F. H. Stillinger, and S. Torquato, Phys. Rev. E **79**, 041309 (2009).
[37] Y. Jiao and S. Torquato, J. Chem. Phys. **135**, 151101 (2011).
[38] S. Torquato and F. H. Stillinger, Experimental Math. **15**, 307 (2006).
[39] C. E. Zachary and S. Torquato, J. Stat. Mech.: Theory and Experiment, P10017 (2011).
[40] S. Torquato and Y. Jiao, Nature **460**, 876 (2009).
[41] S. Torquato and Y. Jiao, Phys. Rev. E **80**, 041104 (2009).